Thermoelectric properties of SnSe nanoribbons: a theoretical aspect



2016 Mater. Res. Express 3 035013

(http://iopscience.iop.org/2053-1591/3/3/035013)

Materials Research Express

PAPER

# Thermoelectric properties of SnSe nanoribbons: a theoretical aspect

**Kriti Tyagi**[1,2], **Kevin Waters**[3], **Gaoxue Wang**[3], **Bhasker Gahtori**[1], **D Haranath**[1] **and Ravindra Pandey**[3]

[1] CSIR-Network of Institutes for Solar Energy, CSIR-National Physical Laboratory, Dr K. S. Krishnan Marg, New Delhi-110012, India
[2] Academy of Scientific and Innovative Research (AcSIR), CSIR-National Physical Laboratory (NPL) Campus, New Delhi, 110012, India
[3] Department of Physics, Michigan Technological University, Houghton, MI, 49931, USA

**E-mail:** tyagikt@nplindia.org, kwaters@mtu.edu **and** gaoxuew@mtu.edu

**RECEIVED**
30 October 2015

**REVISED**
25 February 2016

**ACCEPTED FOR PUBLICATION**
3 March 2016

**PUBLISHED**
18 March 2016

**Keywords:** thermoelectric, density functional theory, materials properties

Supplementary material for this article is available online

## Abstract

Bulk SnSe is reported to be an excellent thermoelectric material at high temperatures. We now present the results on thermoelectric properties of nanoribbons of SnSe of variable widths obtained using density functional theory coupled with semi-classical Boltzmann theory. The calculated results find armchair nanoribbons of width $\leqslant$47 Å to be semiconducting and zigzag nanoribbons of width $\leqslant$52 Å to be metallic. A relatively high Seebeck coefficient ($\approx$1720 $\mu$V K$^{-1}$) and low thermal conductivity was calculated for the armchair nanoribbon of 6 Å width, while a large relaxation time and small effective mass was obtained for the armchair nanoribbon of 47 Å width. The calculated results suggest that patterning SnSe into nanoribbons may provide thermoelectric performance that is similar to the monolayer and low-temperature bulk phases of SnSe.

## 1. Introduction

Thermoelectric materials have the capability to convert waste heat directly into electricity, hence, this class of materials is rapidly emerging as an alternate solution to the ever existing problem of energy crisis. The material's dimensionless figure-of-merit, $ZT = \frac{S^2\sigma T}{\kappa_e + \kappa_l}$, is the key parameter indicating the efficiency of thermoelectric properties, which depends on the Seebeck coefficient ($S$), electrical conductivity ($\sigma$), electronic thermal conductivity ($\kappa_e$), lattice thermal conductivity ($\kappa_l$), and temperature ($T$). By tuning these electronic and thermal properties, researchers aim to enhance the material's figure-of-merit. Alternatively, scaling the material down to nano-sized dimensions is suggested to enhance the power factor ($S^2\sigma$) values [1, 2], due mainly to quantum confinement effects and a reduction in thermal conductivity [3, 4]. The nano-sized structures generally show electronic properties that differ from their bulk counterparts [5–7].

Tin selenide (SnSe) is a group IV–VI semiconducting material that has unique electronic and optical properties due to its layered structure [8, 9]. It has an orthorhombic crystal structure at ambient conditions with a band gap of $\approx$0.90 eV which is suitable for its use in photovoltaic devices [10–12]. Additionally, the thermoelectric properties of the bulk SnSe has been found to be excellent at high temperatures. Specifically, the $ZT$ values at 923 K are reported to be ~2.6, 2.3, and 0.8 along the crystallographic axes $b$, $c$ and $a$ (interlayer), respectively [13] . This is mainly a consequence of the phase transition of SnSe around 750 K from the Pnma to the Cmcm phase [13]. For the polycrystalline SnSe, an average $ZT$ value of 0.5 at 823 K was measured [14]. Recent calculations show that bulk SnSe has a maximum figure of merit of around 1.0 for both n-type and p-type carriers at 300 K and 0.9 at 600 K [15]. At a higher temperature of 750 K, the maximum figure of merit was calculated to be 0.8 for p-type and 1.5 for n-type SnSe [16].

It has recently been reported that a monolayer sheet of SnSe can exhibit a higher lattice thermal conductivity ($\approx$2.3 W mK$^{-1}$ at 300 K [17]) than its bulk counterpart ($\approx$0.7 W mK$^{-1}$ at 300 K in experiment [13] and a calculated 0.32 W mK$^{-1}$ at 300 K [15]). Considering that nanoribbons of SnSe may have lower thermal conductivity relative to the bulk, we embark upon a detailed investigation of thermoelectric properties of

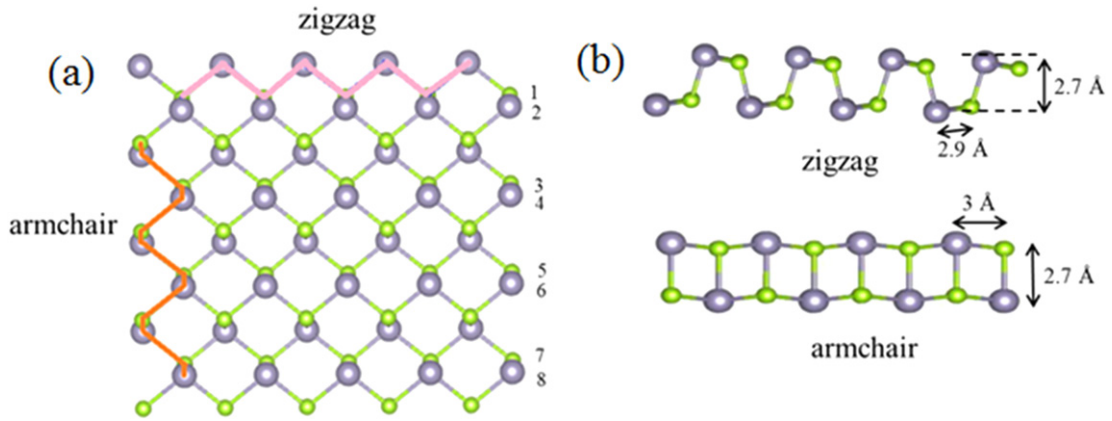


**Figure 1.** (a) Ball and stick model of top view of the structure of the 8-SnSe nanoribbon depicting armchair and zigzag edges. The blue and green spheres represents Sn and Se atom, respectively. (b) Side views of each is given with the bond lengths of each type of Sn–Se bond.

nanoribbons of SnSe calculating their energy band structures, and derived properties in the framework of density functional theory together with the semi-classical Boltzmann theory.

## 2. Computational method

Electronic structure calculations based on density functional theory (DFT), using the Vienna *Ab initio* simulation package (VASP), were performed. A plane-wave basis set together with the project augmented wave pseudopotentials were used. The generalized gradient approximation (GGA) was used in the form of the PW-91 functional [18]. The convergence threshold were $10^{-5}$ eV, $3 \times 10^{-2}$ eV Å$^{-1}$ for energy and force, respectively. An energy cut-off value of 500 eV was used for the plane-wave basis set.

Nanoribbons of SnSe were constructed from a single layer of the bulk orthorhombic structure (Pnma). The calculated values of lattice constants are in good agreement with the experimental values of $a = 11.501$ Å, $b = 4.153$ Å and $c = 4.445$ Å [19]. In the supercell representing a typical nanoribbon configuration, a vacuum region of 10 Å was used to minimize interactions between the periodic images during calculations. A Monkhorst-Pack Scheme with k-point grid of $(4 \times 4 \times 12)$, $(1 \times 1 \times 13)$, $(1 \times 13 \times 1)$ were used for bulk, armchair, and zigzag nanoribbons, respectively. For the electron transport calculations [20–22], a $(3 \times 3 \times 13)$ $k$-point grid was used for the ANRs.

The Seebeck coefficient ($S$), electrical conductivity ($\sigma$), and electronic thermal conductivity ($\kappa_e$) were obtained by the semi-classical Boltzmann theory implemented in the BoltzTrap code [20], which uses details from the VASP calculated band structure. The lattice thermal conductivity ($\kappa_l$) was obtained using the ShengBTE [23–25] program which solves the phonon Boltzmann transport equation. The input files for the ShengBTE program include the second-order interatomic force constants and third-order interatomic force constants. The PHONOPY [26] program was used for the second-order interatomic force constants. The third-order interatomic force constants were obtained by the finite displacement method by moving two atoms in the supercell simultaneously and collecting the force on rest atoms [23]. Note that $\kappa_l$ of the one dimensional nanoribbon is derived from the two-dimensional SnSe monolayer by considering that the boundary scattering rate is a function of the width of the ribbon.

## 3. Results and discussion

Nanoribbons of SnSe can be classified by the direction of termination, and are referred to as armchair ($N$-ANR) and zigzag ($N$-ZNR) nanoribbons with $N$ being the number of edge atoms. Figure 1 illustrates the formation of armchair and zigzag nanoribbons from a SnSe monolayer sheet. The armchair nanoribbon comprises of Sn and Se atoms arranged in an alternative manner along the edges, while the edge of zigzag nanoribbon consists solely of Sn or Se atoms. This arrangement of zigzag nanoribbons is proven to be energetically favourable [27, 28], and is found to be non-magnetic.

The widths of the armchair nanoribbons are 6.1 Å, 14.2 Å, 30.3 Å, 47.1 Å for $N = 4, 8, 16, 24$, respectively. The widths of zigzag nanoribbons are 7.6 Å, 16.1 Å, 31.2 Å, 52.7 Å for $N = 4, 8, 16, 24$, respectively. Note that the equilibrium configurations of SnSe nanoribbons show a few differences from the bulk SnSe in terms of bond

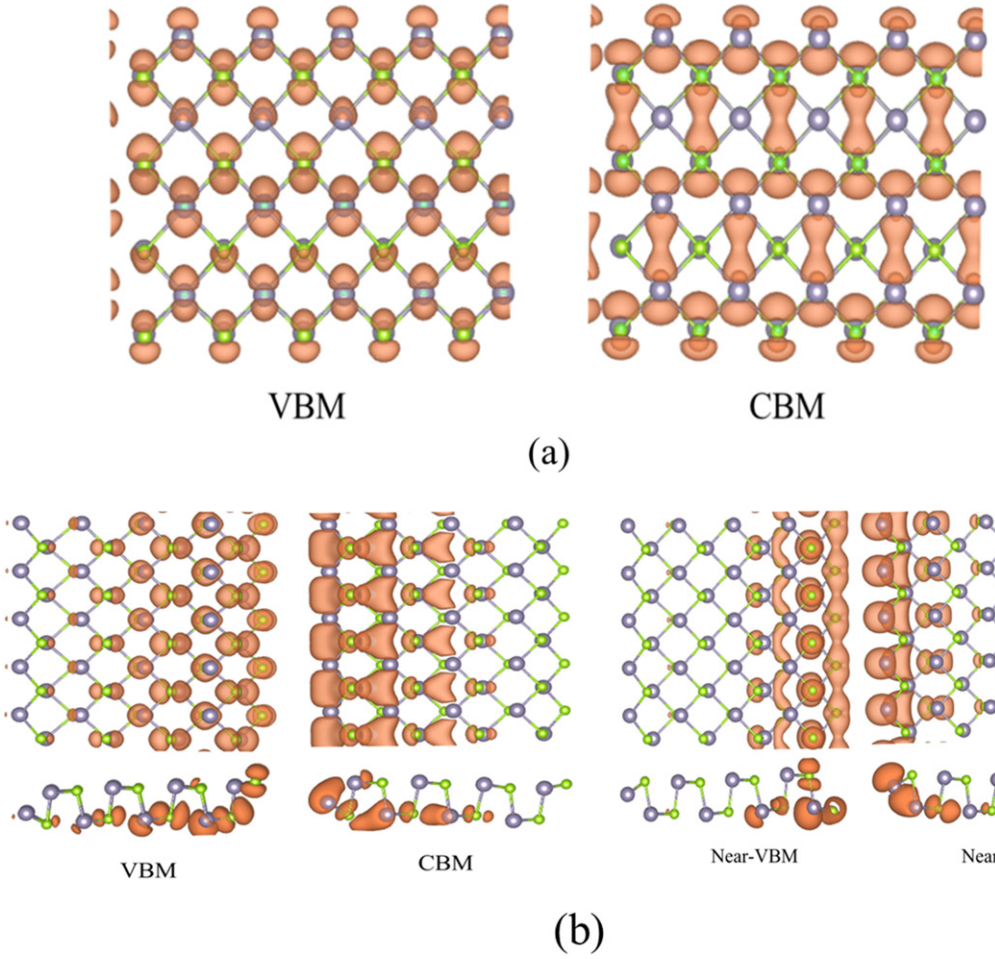


**Figure 2.** Top and side views of the calculated projected charge densities of valence band maximum (VBM) and conduction band minimum (CBM) (a) 8-armchair and (b) 8-zigzag nanoribbons, respectively. Blue and green spheres represents Sn and Se atom, respectively.

lengths. For example, $R_{Sn-Se}$ of the edge atoms associated with 8-ANR (8-ZNR) are 2.7 (2.7) Å and 3.0 (2.9) Å (figure 1) whereas a layered structure of the bulk SnSe has two types of Sn-Se bonds with bond-lengths of 2.7 Å (upright) and 2.8 Å (lateral).

In a recent theoretical investigation based on density functional theory, electronic properties of zigzag (width $<$25 Å) and armchair (width $<$28 Å) nanoribbons of SnSe were reported [29]. It was found that the armchair nanoribbons are semiconducting and the pristine zigzag nanoribbons are metallic. Our calculated results considering the ribbon width of $\approx$50 Å for both zigzag and armchair SnSe nanoribbons are in excellent agreement with the previous results [29]. For example, the calculated binding energy is about 4.05 (4.02) eV atom$^{-1}$ for 24-ANR of width 47 Å and 24-ZNR of width 53 Å, respectively (table S1, supplementary information). The calculated stability increases with the increase in the ribbon width (figure S1, supplementary information). Also, the difference in the binding energies of ANRs and ZNRs reduces with the increase in ribbon width with ANRs being relatively stable.

The ANRs and ZNRs show dissimilar electronic properties. (figures S2 and S3, supplementary information). Armchair nanoribbons of SnSe are semiconducting with an indirect band gap; the calculated bandgap is 0.92 eV for the ribbon width of 47 Å ($N = 24$). Zigzag nanoribbons are metallic with a finite density of states at the Fermi level, and their metallic nature does not depend upon the ribbon width. We note that ZNRs with broken bonds (i.e. D structure) are reported to show an opening of the band gap for $N \geqslant 8$ [29]. Our results are in accordance with those reported for armchair $MoS_2$ [30] as well as grapheme [31] and silicon nanoribbons [32] in terms of the dependence of stability and band gap on the ribbon width.

The calculated results in terms of the projected density of states and the projected charge densities for the valence band maximum (VBM) and the conduction band minimum (CMB) show dissimilarity in their composition and nature associated with ANRs and ZNRs (figure 2 and figure S3, supplementary information). Both the VBM and the CBM are composed of states that are localized on the atoms over the ribbon for the ANRs. In the ZNRs the VBM consists of localized states and the CBM is composed of the delocalized states. The states

**Table 1.** Calculated values of the deformation potential ($E_1$), stretching modulus ($C_{1D}$), effective mass ($m_e$), relaxation time ($\tau$), and lattice thermal conductivity ($\kappa_l$ @ 300 K) for semiconducting armchair SnSe nanoribbons.

| N-ANRs | Width | Carriers | $E_1$ (eV) | $C_{1D}$ (eV Å$^{-1}$) | $m_e$ ($m_0$) | $\tau$ (fs) | $\kappa_L$ (W mK$^{-1}$) |
|---|---|---|---|---|---|---|---|
| 4 | 6.1 Å | Electrons | −4.3.0 | 12.46 | 0.22 | 6.53 | 0.20 |
| | | Holes | −2.08 | 12.46 | 0.42 | 19.95 | |
| 8 | 14.2 Å | Electrons | −5.56 | 29.82 | 0.27 | 8.38 | 0.30 |
| | | Holes | −5.00 | 29.82 | 0.33 | 9.34 | |
| 16 | 30.3 Å | Electrons | −6.49 | 70.07 | 0.15 | 19.48 | 0.42 |
| | | Holes | −5.9.0 | 70.07 | 0.16 | 22.76 | |
| 24 | 47.1 Å | Electrons | −5.17 | 107.6 | 0.13 | 19.70 | 0.50 |
| | | Holes | −8.23 | 107.6 | 0.11 | 55.57 | |

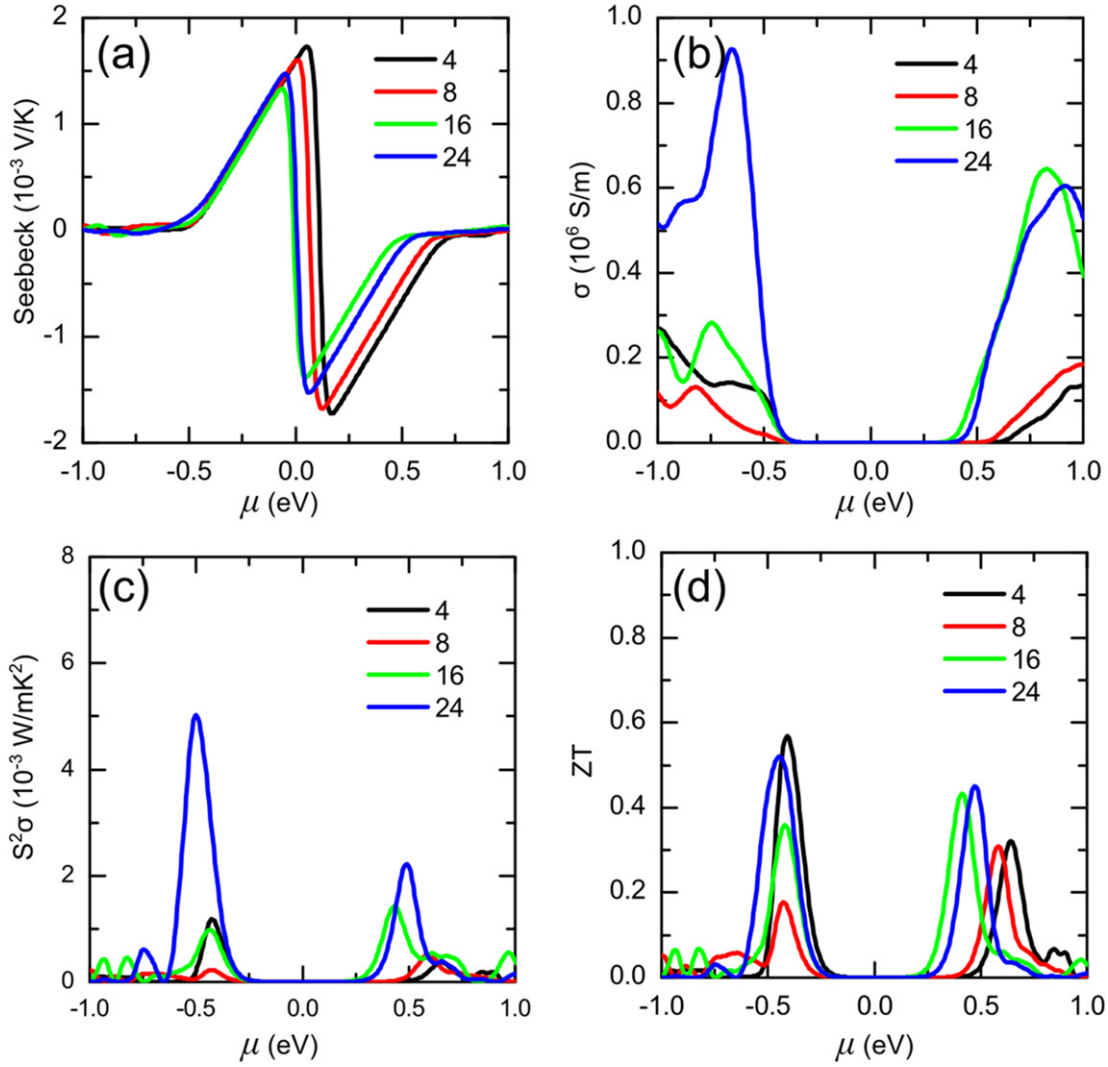


**Figure 3.** Calculated (a) Seebeck coefficient, (b) electrical conductivity, (c) power factor, and (d) *ZT* as a function of chemical potential for 4, 8, 16, and 24-ANRs at 300 K.

for both the CBM and the VBM are localized at the edge of the ribbon. The difference in nature of the CBM states is likely to be the cause of difference in semiconducting or metallic- nature of the SnSe nanoribbons.

An insight into the transport coefficients is obtained using the Boltzmann transport theory as implemented in the BoltzTraP code [20]. The electrical conductivity and electronic thermal conductivity, which are dependent on the relaxation time $\tau$, is approximated using deformation potential theory [33],

$$\tau = \frac{\hbar^2 C_{1D}}{\sqrt{2\pi k_B T}\sqrt{m_e}\,E_1{}^2}, \quad (1)$$

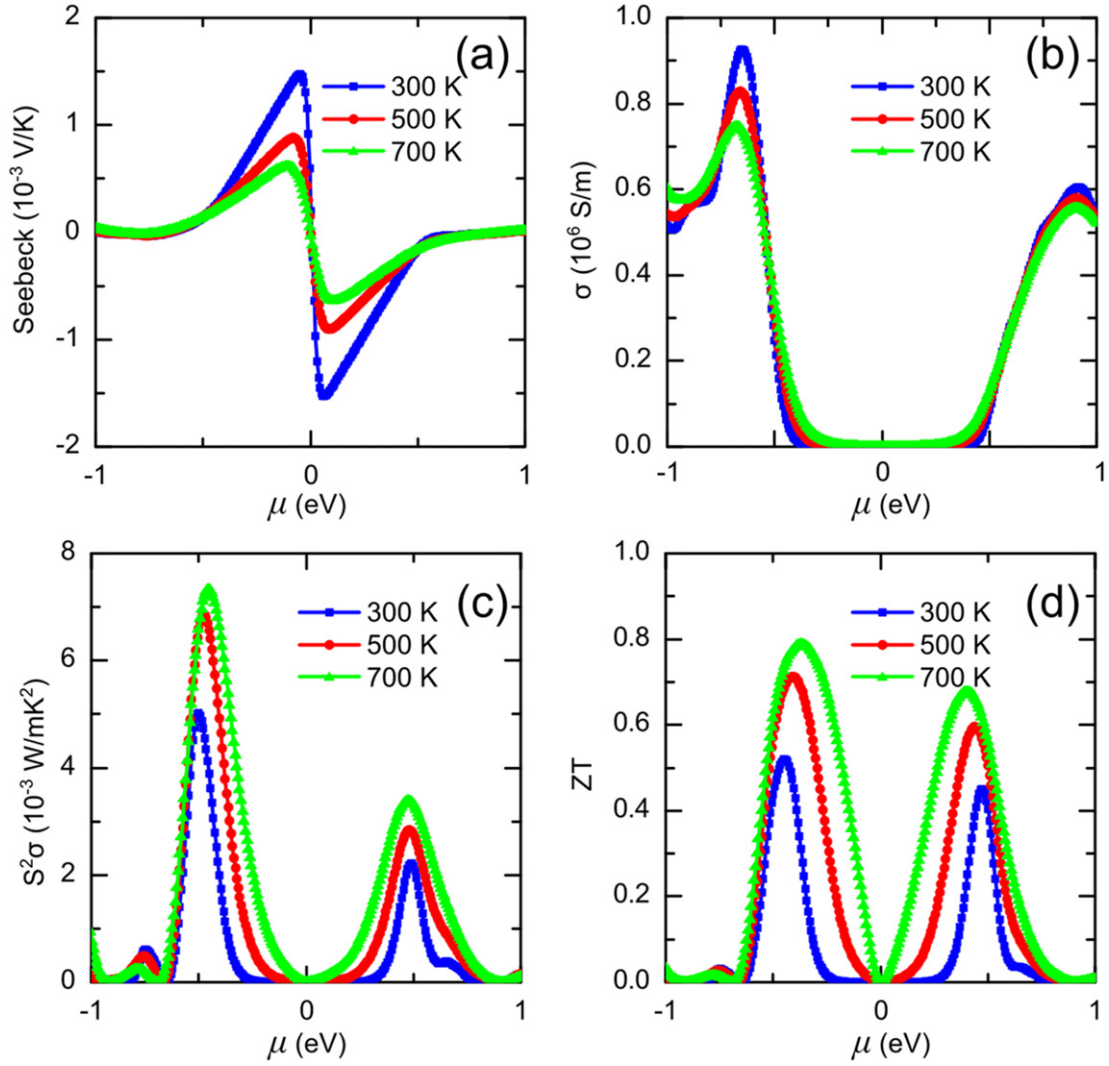


**Figure 4.** SnSe 24-ANR: Calculated (a) Seebeck coefficient, (b) electrical conductivity, (c) power factor, and (d) *ZT* as a function of chemical potential at 300 K, 500 K, and 700 K.

where $C_{1D}$ is the stretching modulus, $E_1$ is the deformation potential, $m_e$ is the effective mass, $e$ is the electronic charge, $\hbar$ is the reduced Planck's constant, $k_B$ is the Boltzmann constant and $T$ is the absolute temperature.

The deformation potential is obtained by applying strain along the nanoribbons and checking the change of the band energy. Figure S4 gives one example for the calculation of $E_1$ for the 24-ANR of SnSe. The stretching modulus $C_{1D}$ is calculated using the equation $C_{1D} = \frac{1}{l_0}\frac{\partial^2 E}{\partial(\Delta l / l_0)^2}$ with $E$ being the strain energy of the ribbons. The effective mass is calculated from the band structures of the nanoribbons using the equation, $m_e = \hbar^2\left(\frac{\partial^2 E(k)}{\partial k^2}\right)^{-1}$.

Table 1 summarizes the calculated results for different widths of ANRs of SnSe. Figure S5 in the supplementary section displays the variation of $\kappa_l$, calculated at 300 K, as a function of width. The calculated lattice thermal conductivity of the armchair SnSe nanoribbons (≈0.2–0.5 W mK$^{-1}$) are smaller than that of the 2D SnSe sheet (≈1.0 W mK$^{-1}$ along the armchair direction) which may be due to the increased phonon scatting at the edges of SnSe nanoribbons.

The calculated $S$, $\sigma$, $S^2\sigma$ and $ZT$ are shown in figure 3 as a function of chemical potential ($\mu$) for different nanoribbons, where $\mu$ is negative for p-type doping and positive for n-type doping in SnSe. A large value of $S$ is noticed for the 4-ANR, which decreases as the width of nanoribbon is increased. This is in agreement with values of the band gap; 4-ANR has a large bandgap which decreases with increasing width of nanoribbons. The maximum value of $S$ for the 4-ANRs is 1720 $\mu$V K$^{-1}$, which is larger than the reported value for the SnSe sheet [17]. On the other hand, $\sigma$ shows an inverse behaviour wherein the highest value is attained for 24-ANR of SnSe. This behaviour can be attributed to a large relaxation time and small effective mass associated with 24-ANR (table 1).

Figure 3(d) displays variation of $ZT$ with the chemical potential for armchair SnSe nanoribbons at 300 K. For p-type doping, the $ZT$ value of 4-ANR reaches about 0.6, while, for n-type doping, $ZT$ is about 0.3. The highest value of $ZT$ for 4-ANRs can be attributed to its relatively high Seebeck coefficient and low thermal conductivity (table 1).

Figure 4 shows temperature dependent thermoelectric properties of the 24-ANR; $S$ decreases with increasing temperature, while $\sigma$ shows the opposite trend. $S^2\sigma$ and $ZT$ values increase with temperature near the band gap. The value of $ZT$ at 700 K is around 0.8 which is comparable to the range of ≈0.2–0.8 for the SnSe sheet at 750 K [17]. $ZT$ for bulk SnSe was measured to be as high as 0.6 at 750 K for p-type doping [34]. A large value of $ZT$ for SnSe nanoribbons may be associated with an increase of the Seebeck coefficient, similar to the case of SnSe monolayer [17].

## 4. Summary

The stability, electronic and transport properties of SnSe nanoribbons are investigated in the framework of density functional theory coupled with semi-classical Boltzmann theory. The calculated results find armchair nanoribbons of width $\leqslant$47 Å to be semiconducting and zigzag nanoribbons of width $\leqslant$52 Å to be metallic. A noticeable difference in nature of conduction band states is likely to be the cause of difference in electronic properties of armchair and zigzag SnSe nanoribbons. The thermoelectric properties including the Seebeck coefficient, electrical conductivity, thermal conductivity, power factor, and the figure-of-merit for the semiconducting armchair nanoribbons are predicted to be different from the corresponding vales for the low-temperature bulk SnSe. A relatively high Seebeck coefficient (≈1720 $\mu$V K$^{-1}$) and low thermal conductivity was calculated for the armchair nanoribbon of 6 Å width, while a large relaxation time and small effective mass was obtained for the armchair nanoribbon of 47 Å width. The calculated figure-of-merit of nanoribbons is predicted to be comparable to that of the monolayer, and the low-temperature *Pnma* bulk SnSe phase. Dissimilar to other materials, like $MoS_2$ [30] and phosphorene [35] where nanoribbons show superior thermoelectric properties than the corresponding bulk materials, the calculated results for SnSe nanoribbons suggest that patterning SnSe into nanoribbons may provide similar thermoelectric performance to the bulk and monolayer phases.

## Acknowledgments

The results presented in this paper are based on work carried out on high performance computing clusters (Rama and Superior) at Michigan Technological University, Houghton, USA. Thanks to William Slough for his invaluable contribution to this analysis and discussions with Jarvis Loh and Munish Sharma that proved fruitful. KT would also like to acknowledge the financial support from Council of Scientific and Industrial Research (CSIR) in the form of SRF Fellowship and Michigan Technological University.

## References

[1] Hicks L D and Dresselhaus M S 1993 *Phys. Rev.* B **47** 12727–31
[2] Hicks L D and Dresselhaus M S 1993 *Phys. Rev.* B **47** 16631–4
[3] Dresselhaus M S, Dresselhaus G, Sun X, Zhang Z, Cronin S B and Koga T 1999 *Phys. Solid State* **41** 679–82
[4] Heremans J P, Thrush C M and Morelli D T 2004 *Phys. Rev.* B **70** 115334
[5] Park C-H and Louie S G 2008 *Nano Lett.* **8** 2200–3
[6] Lu P, Wu X, Guo W and Zeng X C 2012 *Phys. Chem. Chem. Phys.* **14** 13035–40
[7] Botello-Méndez A R, López-Urías F, Terrones M and Terrones H 2008 *Nano Lett.* **8** 1562–5
[8] Seo J-W, Jang J-T, Park S-W, Kim C, Park B and Cheon J 2008 *Adv. Mater.* **20** 4269–73
[9] Choi J, Jin J, Jung I G, Kim J M, Kim H J and Son S U 2011 *Chem.Commun.* **47** 5241–3
[10] Liu S, Guo X, Li M, Zhang W-H, Liu X and Li C 2011 *Angew. Chem. Int. Ed.* **50** 12050–3
[11] Antunez P D, Buckley J J and Brutchey R L 2011 *Nanoscale* **3** 2399–411
[12] Baumgardner W J, Choi J J, Lim Y-F and Hanrath T 2010 *J. Am. Chem. Soc.* **132** 9519–21
[13] Zhao L-D, Lo S-H, Zhang Y, Sun H, Tan G, Uher C, Wolverton C, Dravid V P and Kanatzidis M G 2014 *Nature* **508** 373–7
[14] Sassi S, Candolfi C, Vaney J-B, Ohorodniichuk V, Masschelein P, Dauscher A and Lenoir B 2014 *Appl. Phys. Lett.* **104** 212105
[15] Ding G, Gao G and Yao K 2015 *Sci. Rep.* **5** 9567
[16] Guo R, Wang X, Kuang Y and Huang B 2015 *Phys. Rev.* B **92** 115202
[17] Ding G, Gao G and Yao K 2015 arXiv:1509.01759
[18] Perdew J P, Chevary J A, Vosko S H, Jackson K A, Pederson M R, Singh D J and Fiolhais C 1992 *Phys. Rev.* B **46** 6671–87
[19] Kutorasinski K, Wiendlocha B, Kaprzyk S and Tobola J 2015 *Phys. Rev.* B **91** 205201
[20] Madsen G K H and Singh D J 2006 *Comput. Phys. Commun.* **175** 67–71
[21] Løvvik O M and Prytz Ø 2004 *Phys. Rev.* B **70** 195119
[22] Hedin L and Lundqvist B I 1971 *J. Phys. C: Solid State Phys.* **4** 2064
[23] Li W, Carrete J, Katcho N A and Mingo N 2014 *Comput. Phys. Commun.* **185** 1747–58
[24] Omini M and Sparavigna A 1995 *Physica* B **212** 101–12
[25] Li W, Mingo N, Lindsay L, Broido D, Stewart D A and Katcho N 2012 *Phys.Rev.* B **85** 195436

[26] Togo A and Tanaka I 2015 *Scr. Mater.* **108** 1–5
[27] Deng J, Fampiou I, Liu J Z, Ramasubramaniam A and Medhekar N V 2012 *Appl. Phys. Lett.* **100** 251906
[28] Qi Z, Cao P and Park H S 2013 *J. Appl. Phys.* **114** 163508
[29] Huang Y, Ling C, Liu H and Wang S 2014 *RSC Adv.* **4** 6933–8
[30] Fan D D, Liu H J, Cheng L, Jiang P H, Shi J and Tang X F 2014 *Appl. Phys. Lett.* **105** 133113
[31] Zheng H, Wang Z F, Luo T, Shi Q W and Chen J 2007 *Phys. Rev.* B **75** 165414
[32] Pan L, Liu H J, Tan X J, Lv H Y, Shi J, Tang X F and Zheng G 2012 *Phys. Chem. Chem. Phys.* **14** 13588–93
[33] Bardeen J and Shockley W 1950 *Phys. Rev.* **80** 72
[34] Chen C-L, Wang H, Chen Y-Y, Day T and Snyder G J 2014 *J. Mater. Chem.* A **2** 11171
[35] Zhang J, Liu H J, Cheng L, Wei J, Liang J H, Fan D D, Shi J, Tang X F and Zhang Q J 2014 *Sci. Rep.* **4** 6452